PAPER

Check for updates

Tuning proton dissociation energy in proton carrier doped 2D covalent organic frameworks for anhydrous proton conduction at elevated temperature†

Shuhui Chen,[a] Yue Wu,[a] Ying Zhang,[a] Wenxiang Zhang,[a] Yu Fu,[a] Wenbo Huang,[b] Tong Yan[a] and Heping Ma (ID) *[a]

A theoretical and experimental study gives insights into the change of proton dissociation energy of anhydrous proton carriers (phosphoric acid and 1,2,4-triazole) doped in 2D covalent organic frameworks (COFs) with neutral, polar, Lewis base and positively charged sites in their 1D channels. The dielectric properties of proton carrier incorporated COFs were investigated to determine the formation of nanoscale ionic phases in COFs' channels. The proton carrier doped cationic COF exhibits a much higher dielectric constant in the frequency range of 10^3 Hz to 10^7 Hz than other doped COFs, which may arise from the formation of ethidium-biphosphate or ethidium-triazole ion-pairs in charged COF channels. The ion-pairs lined along cationic COFs' channels produce an enhanced proton dissociation degree coupled with a high dielectric response, leading to a new proton conductivity record (2.77×10^{-2} S cm^{-1}) set by the cationic COF among all reported porous materials under anhydrous conditions and elevated temperatures.

Introduction

Elucidating the relationship between proton-conducting materials' microstructure and their proton conducting properties is very important because it is the fundamental principle for property optimization with respect to fuel cells, electrochemical sensors and electrochemical catalysis.[1–4] In recent years, much effort has been devoted to developing efficient proton-conducting materials, including proton-containing polymers, ionic liquids, and nanoporous materials.[5–10] Although these studies choose different substrate materials, they have the same goal of achieving high proton conductivity *via* (1) increasing the number of transportable free protons under applied dc voltage[11,12] and (2) building well-defined ionic channels to reduce the resistance of proton diffusion in the proton conductor.[13–16]

Recently, nanoporous 2D covalent organic frameworks (COFs) have emerged as interesting crystalline proton-

conductive materials because of their diverse crystalline structures, well-defined nanopores and high thermal and chemical stabilities.[17–20] Those COFs have attracted much attention because of their aligned, dense and tunable pores which can provide intrinsic directly ordered and less tortuous proton transport channels. Several pioneering research studies have been reported to improve COF's proton conductivity by doping or anchoring proton-containing carriers such as sulfonic acid,[21,22] water, azoles,[23,24] and phosphoric acid (PA)[25–28] in the pores or on the COF skeletons. Phosphoric acid and azole doped COFs are very interesting because they can achieve high proton conductivity under anhydrous conditions and elevated temperatures.[29,30] Anhydrous proton conductors enable fuel cells to operate at slightly elevated temperatures (100–200 °C), which can increase the activity of catalysts, provide useful waste heat for cogeneration and reduce the size of the radiator.[31–34]

Although PA and azole doped COFs have shown some advantages in anhydrous proton conducting at elevated temperatures, the present proton conductivity (less than 10^{-3} S cm^{-1}) of these proton conductors is still not comparable with that of commercial perfluoro-sulfonic-acid polymers in water (10^{-1} to 10^{-2} S cm^{-1}).[35–37] The main reason may be that the proton dissociation energies of PA and azoles are much higher than that of water in perfluoro-sulfonic-acid polymers. The highly hydrated sulfonic-acid groups in perfluoro polymers possess a high proton dissociation degree, which makes it easy to release protons and achieve high proton conductivity. The

[a]*Shaanxi Key Laboratory of Energy Chemical Process Intensification, School of Chemical Engineering and Technology, Xi'an Jiaotong University, Xi'an, Shaanxi, 710049, P. R. China. E-mail: maheping@mail.xjtu.edu.cn*

[b]*State Key Laboratory of Luminescence and Applications, Changchun Institute of Optics, Fine Mechanics and Physics, Chinese Academy of Sciences, Changchun 130033, P. R. China*

proton dissociation energy for water in perfluoro-sulfonic-acid polymers calculated by density functional theory (DFT) is 3.66 eV, which is less than that of PA (3.86 eV) and 1,2,4-triazole (4.07 eV) (Fig. S1†). The lower proton dissociation energy barrier in the proton conductor can liberate more protons for free migration under applied voltage, which can increase their proton conductivity. Therefore, to maximize the proton conductivity of PA and azole doped COFs, a feasible approach is to reduce their proton dissociation energy in the incorporated COF system.

Herein, we synthesize four targeted 2D COFs with 1D open nanochannels as well-defined proton transport channels. The tunable pore surface properties of COFs allow us to control the interaction between proton carriers (PA and 1,2,4-triazole) and the COF structure and regulate the proton dissociation energy of PA and 1,2,4-triazole in COFs' channels. By introducing Lewis base, polar and cationic sites into 2D COFs, the proton dissociation degree of PA and 1,2,4-triazole in doped COFs can be tuned. The theoretical study gives insights into the change of the proton dissociation energy after doping PA and 1,2,4-triazole in different COFs. Frequency-dependent dielectric functions were used to investigate the dielectric properties of pristine COFs and doped COFs.[38] The evident increase of the dielectric constant in doped COFs indicated the formation of nanoscale ionic phases in the COFs' channels. Interestingly, the doped cationic COF exhibits a higher dielectric constant in the frequency range of 10^3 Hz to 10^7 Hz than other doped COFs, which may arise from the formation of ethidium-biphosphate or ethidium-azole ion-pairs in charged COF channels. The ion-pair containing COF produces an enhanced proton dissociation degree leading to the PA doped COF with a proton conductivity of 2.77×10^{-2} S cm^{-1}, which is among the best performances in reported porous materials under anhydrous conditions and at elevated temperatures.

Results and discussion

The four targeted 2D COFs with neutral, polar, Lewis base and positively charged pore walls were synthesized through a condensation reaction between trigonal 2,4,6-triformylphloroglucinol (TP) aldehyde and trigonal/linear aromatic amine monomers 2,4,6-triaminopyrimidine (TAP), p-phenylenediamine (PD),[39] 2,6-diaminoanthraquinone (DAAQ),[40] and ethidium bromide (EB).[41] Additionally, the irreversible nature of the β-ketoenamine formation reaction can offer COFs high chemical stability in acid as proved by previous reports.[42–45] The completion of the co-condensation reaction was confirmed by Fourier transform infrared (FT-IR) spectroscopy. The FT-IR spectra of TAP-COF, PD-COF, DAAQ-COF and EB-COF are shown in Fig. S2;† the COFs exhibited the absence of characteristic N–H stretching bands of TAP (3102, 3315 cm^{-1}), PD (3194, 3370 cm^{-1}), DAAQ (3328, 3412 cm^{-1}), and EB (3187, 3314 cm^{-1}), and aldehyde group stretching bands of TP (C=O at 1634 cm^{-1}, O=C–H at 2887 cm^{-1}), indicating the high polymerization degree of the COFs. Furthermore, the lack of OH and C=N stretching peaks and the rise of a new C=C stretching peak at 1577 cm^{-1} demonstrate that all COFs exist in

the keto form, rather than the enol form. Scanning electron microscopy (SEM) of EB-COF and TAP-COF revealed that their morphologies were like nanowires, while the morphologies of DAAQ-COF and PD-COF were presented as flower-like (Fig. S3†).

Powder X-ray diffraction (PXRD) analysis was performed to evaluate the crystallinity of the resulting COFs. The obtained PXRD patterns of EB-COF and DAAQ-COF revealed intense diffraction peaks at 3.3° and a broad peak at 27°, assigned to 100 and 001 diffraction planes respectively. The PXRD pattern of PD-COF revealed intense diffraction peaks at 3.6°, assigned to 100 diffraction planes and three minor peaks at 6.0°, 7.0° and 27°. The PXRD analysis of TAP-COF displayed two main characteristic peaks at 10° and 27°, which were assigned to the reflections from 100 and 001 diffraction planes respectively. The peak positions around 27° corresponded to the stacking distances of around 3.3 Å for EB-COF, 3.4 Å for PD-COF, 3.6 Å for DAAQ-COF and 3.5 Å for TAP-COF, respectively. In addition, the (100) peak of EB-COF, PD-COF and DAAQ-COF had a half-maximum full-width values of 0.36°, indicating the high crystallinity of the COF frameworks. In contrast, TAP-COF exhibited moderate crystallinity, as demonstrated by their broadened diffraction peaks.

Geometrical energy minimizations of COF structures were conducted by using the Materials Studio software package and diffraction patterns were simulated in different stacking modes, including eclipsed (AA) and staggered (AB) modes. The experimental PXRDs agreed well with the patterns simulated in an AA-eclipsed mode for PD-COF, TAP-COF and DAAQ-COF. The energy minimization structure of EB-COF was in the offset AA stacking layers, which could avoid cationic pyridinium centers directly aligned on top of each other. Simulated PXRD of COFs with geometrical energy minimization stacking modes matched well with their PXRD patterns, and 1D hexagonal, aligned and dense channels were estimated to have pore sizes of 0.6 nm, 1.4 nm, 2.2 nm and 1.6 nm for TAP-COF, PD-COF, DAAQ-COF and EB-COF, respectively (Fig. 1).

The porosity features of the COFs were investigated by nitrogen adsorption measurement at 77 K. As illustrated in Fig. 2a, b and d, TAP-COF, PD-COF and EB-COF show type-I reversible isotherms, suggesting that these COFs have microporous networks. The nitrogen adsorption isotherms of DAAQ-COF can be assigned to type-IV reversible isotherms, indicative of their mesoporous characteristics. The BET surface areas are 670.3 m^2 g^{-1} for EB-COF, 1163.4 m^2 g^{-1} for DAAQ-COF, 519.0 m^2 g^{-1} for PD-COF and 75.0 m^2 g^{-1} for TAP-COF, respectively. The pore size distributions exhibit dominant pore diameters of 1.66 nm for EB-COF, 2.25 nm for DAAQ-COF, 1.20 nm for PD-COF and 0.67 nm for TAP-COF, which coincide with the theoretical pore sizes of the simulated structures. The pore volumes are 0.35 cm^3 g^{-1} for EB-COF, 0.51 cm^3 g^{-1} for DAAQ-COF, 0.40 cm^3 g^{-1} for PD-COF and 0.20 cm^3 g^{-1} for TAP-COF respectively.

Anhydrous phosphoric acid (PA) and 1,2,4-triazole were chosen as the proton carriers to be doped in COFs because they can act as both proton donors and acceptors under anhydrous conditions. Taking PA doped COFs as an example, after doping with PA, the surface areas of PA@EB-COF, PA@PD-COF, PA@DAAQ-COF and PA@TAP-COF are decreased to 6.9 m^2
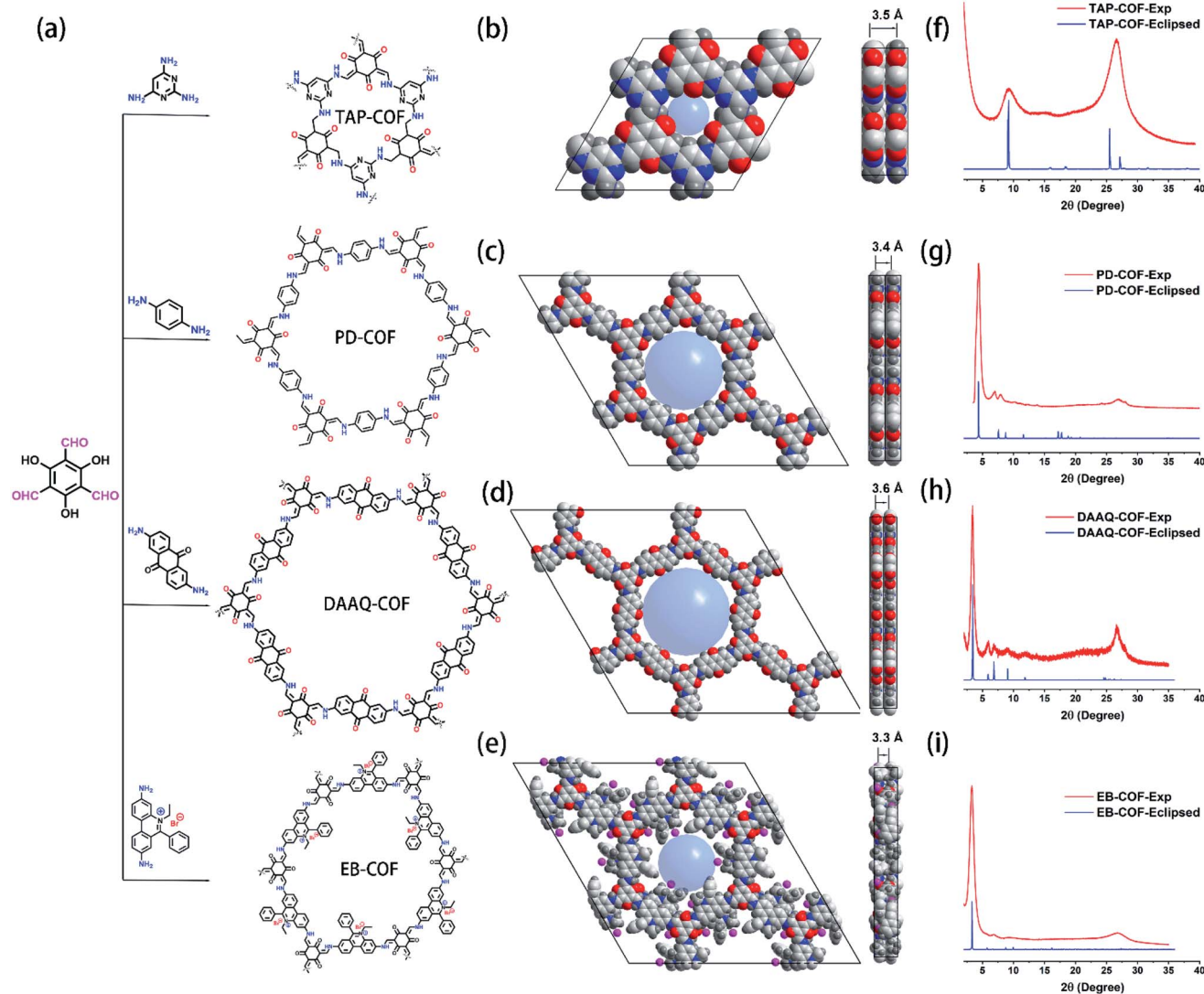
This journal is © The Royal Society of Chemistry 2020

J. Mater. Chem. A, 2020, **8**, 13702–13709 | **13703**

Fig. 1 (a) Synthetic scheme for accessing TAP-COF, PD-COF, DAAQ-COF and EB-COF; (b–e) top and side views of the simulated structure for TAP-COF, PD-COF, DAAQ-COF and EB-COF; (f–i) powder X-ray diffraction spectrum for TAP-COF, PD-COF, DAAQ-COF and EB-COF.

g^{-1}, 0.75 m^2 g^{-1}, 4.0 m^2 g^{-1}, and 13.0 m^2 g^{-1}, respectively, and the pore volumes are only 0.028 cm^3 g^{-1}, 0.03 cm^3 g^{-1}, 0.009 cm^3 g^{-1}, and 0.08 cm^3 g^{-1}, respectively, which mean the PA molecules full filled the channel of the COFs. The EDS mappings (Fig. S4–S7†) of PA@EB-COF, PA@PD-COF, PA@DAAQ-COF and PA@TAP-COF exhibit a homogeneous distribution of phosphoric element throughout the structures. The atomic percentage ratio of P/N for PA@EB-COF, PA@DAAQ-COF, PA@PD-COF and PA@TAP-COF is 1.35, 1.48, 1.10 and 0.48, obtained from the EDS analysis, which means that there are about 13, 8, 6, and 3 PA molecules in the EB-COF, DAAQ-COF, PD-COF and TAP-COF channels respectively. The 1,2,4-triazole loading of tra@EB-COF calculated *via* thermogravimetric (TGA) analysis was 35.1 wt% (Fig. S8d,† carmine curve), which was consistent with the theoretical content of 35.5 wt% calculated *via* pore volume. From TGA analysis (Fig. S8†), we can infer that there are 8, 8, 3, and 1 triazole molecules doped in EB-COF, DAAQ-COF, PD-COF and TAP-COF respectively.

The formation of long-range hydrogen-bonding networks in COF channels can provide continuous proton transfer sites, which is beneficial for the enhancement of proton conduction.[46–48] We use molecular dynamics simulation to elucidate whether the doped PA and 1,2,4-triazole in COFs can form continuous hydrogen-bonding networks. The molecular dynamics simulation results for the hydrogen-bonding interaction in PA and 1,2,4-triazole doped COFs are shown in Fig. 3 and 4. The arrangements of PA and 1,2,4-triazole in COF channels are elucidated by molecular dynamics simulation and the results are shown in the following figures. The first one-layered PA and 1,2,4-triazole are arranged on the pore surface of the COF through O···H and N···H hydrogen bonds resulting from the interaction between PA or triazole and polar groups on the COF frameworks (Fig. S12 and S13†). When more PA and 1,2,4-triazole are loaded in COFs' channel, the subsequent molecules are adsorbed on the first layer *via* hydrogen-bonding (Fig. 3 and 4). Proton carriers and the polar COF structure mean
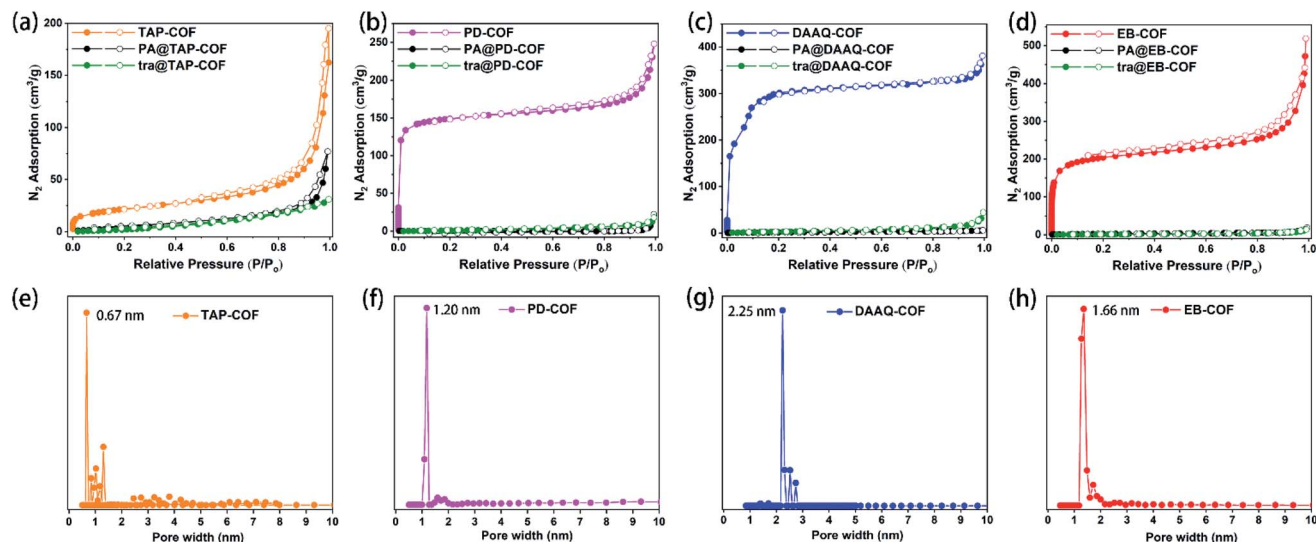
13704 | *J. Mater. Chem. A*, 2020, **8**, 13702–13709

This journal is © The Royal Society of Chemistry 2020

Fig. 2 (a)–(d) Nitrogen sorption isotherms for (a) TAP-COF, (b) PD-COF, (c) DAAQ-COF and (d) EB-COF at 77 K; (e)–(h) pore size distribution of (e) TAP-COF, (f) PD-COF, (g) DAAQ-COF and (h) EB-COF.

the PA and 1,2,4-triazole molecules can arrange along the COFs' 1D channel. Taking PA doped COFs as an example, PA attached on the pore wall of the COF forms long-range correlated hydrogen bonds between COF layers. Protons can rapidly transfer along extended hydrogen bond chains in COF's channel in a confinement domain.

The number of free migrating protons in a proton conducting material is dictated by the releasable protons in the proton source at a given voltage. The proton source with low proton dissociation energy can deliver more protons at a certain voltage. We use density functional theory (DFT) to calculate the proton dissociation energy in our doped COFs. All DFT calculations were performed using the Dmol^3 code in Materials Studio software. The GGA/PBE exchange–correlation functional with the DND basis set was used, and van der Waals correction (DFT-D) was applied. The K-point was set to $1 \times 1 \times 2$ with an orbital global cutoff of 3.7 Å for all atoms.

In PA and 1,2,4-triazole molecules, liberating one proton needs 3.86 eV and 4.07 eV energy. After doping PA in the COF, the proton remains close to the biphosphate anion and produces a relatively weak COF$\cdots$H$\cdot$H$_2$PO$_4$ interaction. Then the proton is much easier to be liberated from PA due to the interaction between the biphosphate anion and COF skeleton. The interaction energy between the COF and biphosphate anion is computed to be 17.4 eV, 12 eV, 23 eV and 123 eV for TAP-COF, PD-COF, DAAQ-COF and EB-COF respectively. Accordingly, the proton dissociation energy is calculated to be 3.68 eV, 3.17 eV, 2.89 eV and 2.38 eV for PA@TAP-COF, PA@PD-COF, PA@DAAQ-COF and PA@EB-COF, respectively (Table 1). It is clear that after doping in the COF, the proton dissociation energy of PA@COF is less than that of pristine PA (3.86 eV). We also calculated the proton dissociation energy of 1,2,4-triazole doped COFs and the results are also listed in Table 1. The considerably low proton dissociation energy values observed for PA and triazole doped cationic EB-COFs are particularly noteworthy (Fig. 5). The
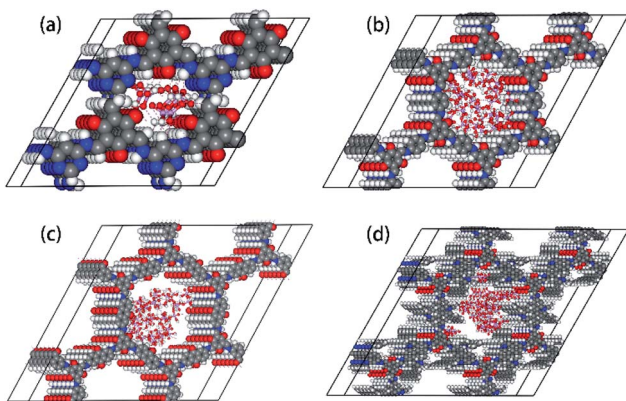

Fig. 3 Graphic representations of PA molecules in the COF channels: (a) TAP-COF, (b) PD-COF, (c) DAAQ-COF and (d) EB-COF (H, white; P, purple; O, red; N, blue; C, gray).
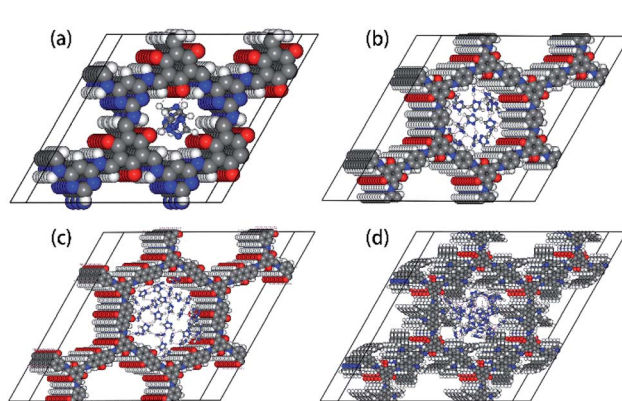

Fig. 4 Graphic representations of 1,2,4-triazole molecules in the COF channels: (a) TAP-COF, (b) PD-COF, (c) DAAQ-COF and (d) EB-COF (H, white; P, purple; O, red; N, blue; C, gray).

This journal is © The Royal Society of Chemistry 2020

J. Mater. Chem. A, 2020, **8**, 13702–13709 | **13705**

Table 1 Proton dissociation energy of PA@COFs and tra@COFs

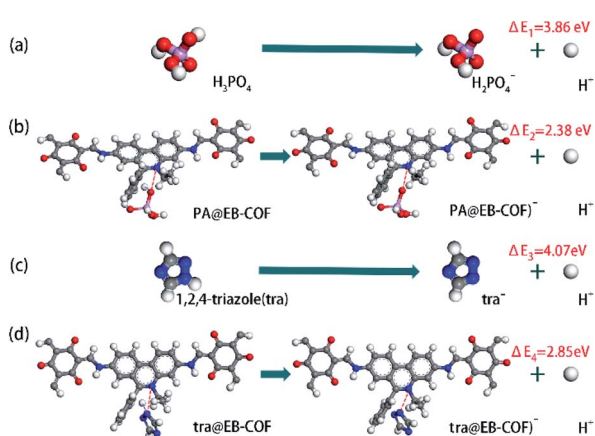| Proton dissociation energy			
Entry	eV	Entry	eV
Phosphoric acid (PA)	3.86	1,2,4-Triazole (tra)	4.07
PA@TAP-COF	3.68	tra@TAP-COF	3.83
PA@PD-COF	3.17	tra@PD-COF	3.66
PA@DAAQ-COF	2.89	tra@DAAQ-COF	3.93
PA@EB-COF	2.38	tra@EB-COF	2.85

Fig. 5 Graphic representations of proton dissociation energy values for (a) PA, (b) PA@EB-COF, (c) 1,2,4-triazole and (d) tra@EB-COF (H, white; P, purple; O, red; N, blue; C, gray).
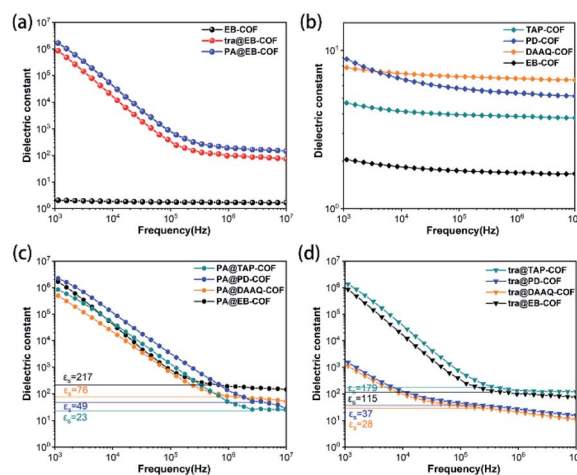

Fig. 6 (a) Dielectric constant of EB-COF (black), tra@EB-COF (red), and PA@EB-COF (blue); (b) dielectric constant of the four target COFs; (c) dielectric constant of PA@COFs; (d) dielectric constant of tra@COFs measured at approximately 10^3–10^7 Hz at 120 °C.

positively charged COF is able to form ion pairs with $H_2PO_4^-$. The strong coulombic interaction between the cationic COF and anionic $H_2PO_4^-$ would significantly decrease the energy barrier of proton dissociation from $H \cdot H_2PO_4$. It has been reported that the interactions driven by quaternary ammonium-biphosphate ion pairs in the polymer can increase their proton conductivity performance at elevated temperature.[49] But the introduced ion pairs into the COF have not, to our knowledge, been explicitly revealed. The ionic pairs confined in the nanoscale channel of the COF could act as both proton donors and acceptors, as well as the dipolar orientational alignment can increase the rate of proton diffusion along nanochannels.

The molecular-level understanding of the ionic pair containing COF is of interest from both fundamental and applied points of view. Therefore, we use the frequency-dependent dielectric function to assess proton and ions interactions in COFs' channel. Fig. 6a displays a representative example of the frequency dependence of the dielectric permittivity $\varepsilon'(\omega)$ for pristine COFs and their corresponding doped COFs. The static dielectric constant ε_s is defined as the low frequency plateau of $\varepsilon'(\omega)$ before the onset of electrode polarization. Remarkably, the doped COFs exhibited higher ε_s than the neat COFs. Considering that ε_s here reflects a response of the dipole moments to the applied electric field, it should be related to the density of dipoles stemming from proton and ionic pairs in COF channels.[50,51] As shown in Fig. 6c, the PA doped EB-COF has a significantly higher dielectric constant (217) than other doped

COFs (23 for PA@TAP-COF, 49 for PA@PD-COF and 76 for PA@DAAQ-COF), which means that it possesses higher number densities of ionic pairs than the PA doped uncharged COFs. It is worth noting that the dielectric constant value of PA doped EB-COF is much larger than that of phosphoric acid ($\varepsilon_s \approx 61$).[52] We speculate that the significantly improved dielectric response of PA@EB-COF mainly originates from ethidium-biphosphate ion pairs involved in intermolecular hydrogen bonding. The same result was also observed for 1,2,4-triazole doped COFs. Notably, the COF with Lewis base and positive charge sites in pores showed a much higher dielectric constant than the COF with neutral and polar pore walls. The higher dielectric constants of PA@COFs and tra@COFs than pristine COFs also suggested that the formation of hydrogen-bonded chains in COF pores as extended hydrogen bonds generally possess high dielectric constants due to cooperative dipole orientation encouraged by hydrogen bonding. The above results revealed that the introduction of PA and 1,2,4-triazole proton carriers into the COF channel can form ion pairs and a long-range hydrogen-bonding network in the channel. Moreover, the high proton dissociation degree of ion pairs in the cationic COF gives rise to a high concentration of intrinsic free protons to transport.

The proton conductivities of the four pristine COFs, PA@COFs and tra@COFs were measured under anhydrous conditions from 80–200 °C by using alternating-current impedance spectroscopy. We found that the proton conductivities of the four pristine COFs were lower than 10^{-10} S cm^{-1} under anhydrous conditions (Fig. S9†), which were thought to be negligible as predicted. Fig. 7 shows the temperature-dependent proton conductivities of COFs with PA and triazole as proton additives, revealing that the proton conductivities decrease in the order of PA@COF > tra@COF > COF, in good agreement with the results of dielectric constant measurements. The proton conductivities of PA@DAAQ-COF, PA@PD-COF and PA@TAP-COF increase while the temperature increases, and then reduce gradually with the rise of
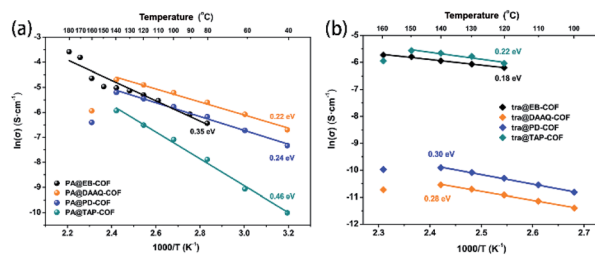
Fig. 7 Temperature dependence of the proton conductivities of (a) PA@COFs and (b) tra@COFs.

temperature, which reach the highest values at a temperature of 140 °C. The maximum values are 9.20×10^{-3} S cm^{-1}, 5.51×10^{-3} S cm^{-1} and 2.65×10^{-3} S cm^{-1} for PA@DAAQ-COF, PA@PD-COF, and PA@TAP-COF respectively, at 140 °C under anhydrous conditions. However, the values rapidly decrease to 2.64×10^{-3} S cm^{-1} and 1.66×10^{-3} S cm^{-1} for PA@DAAQ-COF and PA@PD-COF respectively at 160 °C. The proton conductivities of PA@EB-COF are 1.60×10^{-3}, 2.30×10^{-3}, 3.07×10^{-3}, 3.97×10^{-3}, 4.95×10^{-3}, 5.88×10^{-3}, 6.63×10^{-3}, 6.94×10^{-3}, 9.66×10^{-3}, 2.21×10^{-2}, and 2.77×10^{-2} S cm^{-1} at 80, 90, 100, 110, 120, 130, 140, 150, 160, 170 and 180 °C (Table S2†), respectively, which increases even when the temperature goes up to 180 °C and is comparable with the highest values (1.91×10^{-1} S cm^{-1} for H$_3$PO$_4$@TPB-DMeTP-COF at 160 °C under anhydrous conditions[53]) and exceed that of most previously reported COFs and MOFs (Table 2). The high proton conductivity for PA@EB-COF can be attributed to the formation of ethidium-biphosphate ion-pairs in charged COF skeletons. Just like PA@COFs, the proton conductivities of tra@COFs improve significantly as the temperature increases, and then decrease with the rise of temperature. At 160 °C and 150 °C the proton conductivity values reach a maximum of 3.25×10^{-3} S cm^{-1} for tra@EB-COF and 3.82×10^{-3} S cm^{-1} for tra@TAP-COF, respectively, which are the highest values among the triazole loaded COFs under anhydrous conditions (1.10×10^{-3} S cm^{-1}

for trz@TPB-DMTP-COF at 130 °C under anhydrous conditions[23]). The activation energy (E_a) values for PA@EB-COF, PA@DAAQ-COF, PA@PD-COF and PA@TAP-COF were 0.35 eV, 0.22 eV, 0.24 eV and 0.46 eV respectively calculated from temperature-dependent conductivity data. It is well known that E_a values in the ranges 0.1–0.4 eV and 0.5–0.9 eV reveal Grotthuss mechanisms and vehicular mechanisms, respectively.[54,55] The low E_a value for PA@COF and tra@COF in the high-temperature area may be assigned to the Grotthuss mechanism.

Based on the above experimental and theoretical analysis results, we try to elucidate the relationship between COFs' microstructure and their proton conducting properties in the following two aspects: (1) pore chemical environment. The polar sites in COFs' pore surface such as Lewis base and positive charge sites can enhance the interaction between the COF skeletons and proton carriers. The COF possessing stronger interactions with proton carriers can facilitate the liberation of more protons by proton carriers for free migration, which can increase their proton conductivity; (2) pore size and its matching with proton carriers. Theoretically, the COF with a larger pore size can load more proton carriers, which is beneficial to improve the proton conductivity. However, when the COF's pore size is too wide, the free proton carriers with weak interaction with COF's structure can migrate to one side under the action of an electric field at high temperature, which can lead to the decrease of proton conductivity as observed in PA-doped poly-benzimidazole and our work. So, the pore diameter of the COF should match with the size of proton carriers in a suitable interaction. We find that the introduction of ion-pairs into COF channels is an effective way to improve their proton conductivity. The confined ionic pairs in the nanoscale channel of the COF could act as both proton donors and acceptors, so that they can form extended hydrogen-bond chains in COF's channel. Moreover, the much strong electrostatic interaction between the COF and ionic pairs can avoid the loss of proton carriers and keep the loaded proton carriers and hydrogen-bonding networks stable.

Table 2 List of proton conductivity data of reported COFs and MOFs

Sr. No.	Compound name	Conductivity (S cm^{-1})	E_a (eV)	Conditions	References
1	**PA@EB-COF**	$\mathbf{2.77 \times 10^{-2}}$	**0.35**	**180 °C, anhydrous**	**This work**
	PA@EB-COF	$\mathbf{5.88 \times 10^{-3}}$	**0.35**	**130 °C, anhydrous**	
	PA@DAAQ-COF	$\mathbf{9.20 \times 10^{-3}}$	**0.22**	**140 °C, anhydrous**	
	PA@PD-COF	$\mathbf{5.51 \times 10^{-3}}$	**0.24**	**140 °C, anhydrous**	
	tra@EB-COF	$\mathbf{2.31 \times 10^{-3}}$	**0.18**	**130 °C, anhydrous**	
	tra@EB-COF	$\mathbf{3.25 \times 10^{-3}}$	**0.18**	**160 °C, anhydrous**	
2	phytic@TpPa-Py	3.00×10^{-4}	0.10	120 °C, anhydrous	*Chem. Mater.*, 2016, **28**, 1489 (ref. 18)
	phytic@TpPa-SO$_3$H	7.50×10^{-5}	0.16	120 °C, anhydrous	
3	PA@TpBpy-MC	2.50×10^{-3}	0.11	120 °C, anhydrous	*J. Mater. Chem. A*, 2016, **4**, 2682 (ref. 28)
	PA@TpBpy-ST	1.98×10^{-3}	0.12	120 °C, anhydrous	
4	Im@TPB-DMTP-COF	4.37×10^{-3}	0.38	130 °C, anhydrous	*Nat. Mater.*, 2016, **15**, 722 (ref. 23)
	trz@TPB-DMTP-COF	1.10×10^{-3}	0.21	130 °C, anhydrous	
5	Im@Td-PPI$_2$	3.49×10^{-4}	0.30	90 °C, anhydrous	*J. Am. Chem. Soc.*, 2015, **137**, 913 (ref. 24)
6	PA@Tp-Azo	6.7×10^{-5}	0.11	67 °C, anhydrous	*J. Am. Chem. Soc.*, 2014, **136**, 6570 (ref. 27)
7	[ImH$_2$] [Cu(H$_2$PO$_4$)$_{1.5}$(HPO$_4$)$_{0.5}$Cl$_{0.5}$]	2.0×10^{-2}	1.10	130 °C, anhydrous	*Chem. Commun.*, 2014, **50**, 10241 (ref. 56)
8	[Zn$_3$(H$_2$PO$_4$)$_6$] (Hbim)	1.3×10^{-3}	0.50	120 °C, anhydrous	*J. Am. Chem. Soc.*, 2013, **135**, 11345 (ref. 57)
9	H$_3$PO$_4$@TPB-DMeTP-COF	1.91×10^{-1}	0.34	160 °C, anhydrous	*Nat. Commun.*, 2020, **11**, 1981 (ref. 53)

This journal is © The Royal Society of Chemistry 2020

J. Mater. Chem. A, 2020, **8**, 13702–13709 | **13707**

Conclusions

In summary, by introducing neutral, polar, Lewis base and cationic sites into the 2D COFs' pore wall, the proton dissociation degree of PA and 1,2,4-triazole can be tuned in the doped COFs. Moreover, the alignment of PA and 1,2,4-triazole along COFs' 1D channel can form long-range hydrogen-bonding networks, which can provide continuous proton transfer channels. The dielectric properties of proton carrier incorporated COFs were investigated to determine the formation of ionic phases in COFs' channels. Compared with the pristine COFs, the PA and 1,2,4-triazole loaded COFs exhibit excellent proton conductivities in the temperature range from 80 °C to 200 °C under anhydrous conditions. The proton conductivity value of 2.77×10^{-2} S cm^{-1} of PA@EB-COF is ranked among the highest values of reported porous materials due to the formation of ethidium-biphosphate ion-pairs in charged COF channels. The ion-pairs lined along the channels of the cationic COF can decrease proton dissociation energy and act as proton transfer sites simultaneously. Based on the detailed comparison of the PA and 1,2,4-triazole doped COFs, we find out that the chemical properties of the pore wall play an important role in improving the proton conductivity of porous materials. The COFs possessing strong interaction with proton carriers could promote proton release from carriers under applied voltage, which can increase their proton conductivities. We believe that our findings will provide better understanding of structure–conductivity relationships and help develop stable and efficient COF-based proton conducting materials at high temperature.

Conflicts of interest

There are no conflicts to declare.

Acknowledgements

Notes and references

1 Q. Li, J. O. Jensen, R. F. Savinell and N. J. Bjerrum, *Prog. Polym. Sci.*, 2009, **34**, 449–477.
2 G. He, M. Xu, J. Zhao, S. Jiang, S. Wang, Z. Li, X. He, T. Huang, M. Cao and H. Wu, *Adv. Mater.*, 2017, **29**, 1605898.
3 J. Le Bideau, L. Viau and A. Vioux, *Chem. Soc. Rev.*, 2011, **40**, 907–925.
4 J. Wu, F. Xu, S. Li, P. Ma, X. Zhang, Q. Liu, R. Fu and D. Wu, *Adv. Mater.*, 2019, **31**, 1802922.
5 Y. Wu, D. Yan, Z. Zhang, M. M. Matsushita and K. Awaga, *ACS Appl. Mater. Interfaces*, 2019, **11**, 7661–7665.
6 W. Kong, W. Jia, R. Wang, Y. Gong, C. Wang, P. Wu and J. Guo, *Chem. Commun.*, 2019, **55**, 75–78.
7 D. W. Kang, K. S. Lim, K. J. Lee, J. H. Lee, W. R. Lee, J. H. Song, K. H. Yeom, J. Y. Kim and C. S. Hong, *Angew. Chem., Int. Ed.*, 2016, **55**, 16123–16126.
8 S. Wang, Q. Wang, P. Shao, Y. Han, X. Gao, L. Ma, S. Yuan, X. Ma, J. Zhou and X. Feng, *J. Am. Chem. Soc.*, 2017, **139**, 4258–4261.
9 J. F. Wu and X. Guo, *Small*, 2019, **15**, 1804413.
10 K. Fujie, R. Ikeda, K. Otsubo, T. Yamada and H. Kitagawa, *Chem. Mater.*, 2015, **27**, 7355–7361.
11 C. Montoro, D. Rodríguez-San-Miguel, E. Polo, R. Escudero-Cid, M. L. Ruiz-González, J. A. Navarro, P. Ocón and F. L. Zamora, *J. Am. Chem. Soc.*, 2017, **139**, 10079–10086.
12 B. Zhou, J. Le, Z. Cheng, X. Zhao, M. Shen, M. Xie, B. Hu, X. Yang, L. Chen and H. Chen, *ACS Appl. Mater. Interfaces*, 2020, **12**, 8198–8205.
13 Z. Wang, R. Tan, H. Wang, L. Yang, J. Hu, H. Chen and F. Pan, *Adv. Mater.*, 2018, **30**, 1704436.
14 Y. Yoshida, K. Fujie, D. W. Lim, R. Ikeda and H. Kitagawa, *Angew. Chem., Int. Ed.*, 2019, **58**, 10909–10913.
15 K. Fujie and H. Kitagawa, *Coord. Chem. Rev.*, 2016, **307**, 382–390.
16 K.-D. Kreuer, *Chem. Mater.*, 2014, **26**, 361–380.
17 J. A. Hurd, R. Vaidhyanathan, V. Thangadurai, C. I. Ratcliffe, I. L. Moudrakovski and G. K. Shimizu, *Nat. Chem.*, 2009, **1**, 705–710.
18 S. Chandra, T. Kundu, K. Dey, M. Addicoat, T. Heine and R. Banerjee, *Chem. Mater.*, 2016, **28**, 1489–1494.
19 H. Furukawa, K. E. Cordova, M. O'Keeffe and O. M. Yaghi, *Science*, 2013, **341**, 1230444.
20 H. Zhong, Z. Fu, J. M. Taylor, G. Xu and R. Wang, *Adv. Funct. Mater.*, 2017, **27**, 1701465.
21 H. S. Sasmal, H. B. Aiyappa, S. N. Bhange, S. Karak, A. Halder, S. Kurungot and R. Banerjee, *Angew. Chem.*, 2018, **130**, 11060–11064.
22 Y. Peng, G. Xu, Z. Hu, Y. Cheng, C. Chi, D. Yuan, H. Cheng and D. Zhao, *ACS Appl. Mater. Interfaces*, 2016, **8**, 18505–18512.
23 H. Xu, S. Tao and D. Jiang, *Nat. Mater.*, 2016, **15**, 722–726.
24 Y. Ye, L. Zhang, Q. Peng, G.-E. Wang, Y. Shen, Z. Li, L. Wang, X. Ma, Q.-H. Chen and Z. Zhang, *J. Am. Chem. Soc.*, 2015, **137**, 913–918.
25 Z. Meng, A. Aykanat and K. A. Mirica, *Chem. Mater.*, 2018, **31**, 819–825.
26 Y. Yang, X. He, P. Zhang, Y. H. Andaloussi, H. Zhang, Z. Jiang, Y. Chen, S. Ma, P. Cheng and Z. Zhang, *Angew. Chem., Int. Ed.*, 2020, **59**, 3678–3684.
27 S. Chandra, T. Kundu, S. Kandambeth, R. BabaRao, Y. Marathe, S. M. Kunjir and R. Banerjee, *J. Am. Chem. Soc.*, 2014, **136**, 6570–6573.

13708 | *J. Mater. Chem. A*, 2020, **8**, 13702–13709

This journal is © The Royal Society of Chemistry 2020

28 D. B. Shinde, H. B. Aiyappa, M. Bhadra, B. P. Biswal, P. Wadge, S. Kandambeth, B. Garai, T. Kundu, S. Kurungot and R. Banerjee, *J. Mater. Chem. A*, 2016, **4**, 2682–2690.

29 K. C. Ranjeesh, R. Illathvalappil, S. D. Veer, J. Peter, V. C. Wakchaure, Goudappagouda, K. V. Raj, S. Kurungot and S. S. Babu, *J. Am. Chem. Soc.*, 2019, **141**, 14950–14954.

30 L. Wu, Y. Yang, Y. Ye, Z. Yu, Z. Song, S. Chen, L. Chen, Z. Zhang and S. Xiang, *ACS Appl. Energy Mater.*, 2018, **1**, 5068–5074.

31 S. Bose, T. Kuila, T. X. H. Nguyen, N. H. Kim, K.-t. Lau and J. H. Lee, *Prog. Polym. Sci.*, 2011, **36**, 813–843.

32 Q. Li, R. He, J. O. Jensen and N. J. Bjerrum, *Chem. Mater.*, 2003, **15**, 4896–4915.

33 P. Bhanja, A. Palui, S. Chatterjee, Y. V. Kaneti, J. Na, Y. Sugahara, A. Bhaumik and Y. Yamauchi, *ACS Sustainable Chem. Eng.*, 2020, **8**, 2423–2432.

34 K. Wang, L. Yang, W. Wei, L. Zhang and G. Chang, *J. Membr. Sci.*, 2018, **549**, 23–27.

35 C. Ma, L. Zhang, S. Mukerjee, D. Ofer and B. Nair, *J. Membr. Sci.*, 2003, **219**, 123–136.

36 K. A. Mauritz and R. B. Moore, *Chem. Rev.*, 2004, **104**, 4535–4586.

37 A. Kraytsberg and Y. Ein-Eli, *Energy Fuels*, 2014, **28**, 7303–7330.

38 P. Shao, J. Li, F. Chen, L. Ma, Q. Li, M. Zhang, J. Zhou, A. Yin, X. Feng and B. Wang, *Angew. Chem., Int. Ed.*, 2018, **57**, 16501–16505.

39 S. Kandambeth, A. Mallick, B. Lukose, M. V. Mane, T. Heine and R. Banerjee, *J. Am. Chem. Soc.*, 2012, **134**, 19524–19527.

40 C. R. DeBlase, K. E. Silberstein, T.-T. Truong, H. c. D. Abruña and W. R. Dichtel, *J. Am. Chem. Soc.*, 2013, **135**, 16821–16824.

41 H. Ma, B. Liu, B. Li, L. Zhang, Y.-G. Li, H.-Q. Tan, H.-Y. Zang and G. Zhu, *J. Am. Chem. Soc.*, 2016, **138**, 5897–5903.

42 P. Pachfule, A. Acharjya, J. r. m. Roeser, T. Langenhahn, M. Schwarze, R. Schomäcker, A. Thomas and J. Schmidt, *J. Am. Chem. Soc.*, 2018, **140**, 1423–1427.

43 H. B. Aiyappa, J. Thote, D. B. Shinde, R. Banerjee and S. Kurungot, *Chem. Mater.*, 2016, **28**, 4375–4379.

44 S. Karak, S. Kandambeth, B. P. Biswal, H. S. Sasmal, S. Kumar, P. Pachfule and R. Banerjee, *J. Am. Chem. Soc.*, 2017, **139**, 1856–1862.

45 S. Kandambeth, K. Dey and R. Banerjee, *J. Am. Chem. Soc.*, 2018, **141**, 1807–1822.

46 M. Inukai, S. Horike, T. Itakura, R. Shinozaki, N. Ogiwara, D. Umeyama, S. Nagarkar, Y. Nishiyama, M. Malon and A. Hayashi, *J. Am. Chem. Soc.*, 2016, **138**, 8505–8511.

47 O. Kim, K. Kim, U. H. Choi and M. J. Park, *Nat. Commun.*, 2018, **9**, 1–8.

48 L. Vilčiauskas, M. E. Tuckerman, G. Bester, S. J. Paddison and K.-D. Kreuer, *Nat. Chem.*, 2012, **4**, 461.

49 K.-S. Lee, J. S. Spendelow, Y.-K. Choe, C. Fujimoto and Y. S. Kim, *Nat. Energy*, 2016, **1**, 16120.

50 U. H. Choi, A. Mittal, T. L. Price Jr, H. W. Gibson, J. Runt and R. H. Colby, *Macromolecules*, 2013, **46**, 1175–1186.

51 D. Fragiadakis, S. Dou, R. H. Colby and J. Runt, *Macromolecules*, 2008, **41**, 5723–5728.

52 R. A. Munson, *J. Chem. Phys.*, 1964, **40**, 2044–2046.

53 During the submission of our manuscript, Professor Jiang reported proton super flow in COF by confining the H_3PO_4 network in COFs' channels. Their proton conductivity can reach 1.91×10^{-1} S cm^{-1}. S. Tao, L. Zhai, A. D. Wonanke, M. A. Addicoat, Q. Jiang and D. Jiang, *Nat. Commun.*, 2020, **11**, 1981–1987.

54 G. Xing, T. Yan, S. Das, T. Ben and S. Qiu, *Angew. Chem., Int. Ed.*, 2018, **57**, 5345–5349.

55 X. Meng, H.-N. Wang, S.-Y. Song and H.-J. Zhang, *Chem. Soc. Rev.*, 2017, **46**, 464–48056.

56 S. Horike, W. Chen, T. Itakura, M. Inukai, D. Umeyama, H. Asakura and S. Kitagawa, *Chem. Commun.*, 2014, **50**, 10241–10243.

57 D. Umeyama, S. Horike, M. Inukai and S. Kitagawa, *J. Am. Chem. Soc.*, 2013, **135**, 11345–11350.

This journal is © The Royal Society of Chemistry 2020

J. Mater. Chem. A, 2020, **8**, 13702–13709 | **13709**